Piezoelectric MEMS resonators based on ultrathin epitaxial GaN heterostructures on Si

2016 J. Micromech. Microeng. 26 105015

(http://iopscience.iop.org/0960-1317/26/10/105015)

IOP Publishing
Journal of Micromechanics and Microengineering
J. Micromech. Microeng. **26** (2016) 105015 (6pp)
doi:10.1088/0960-1317/26/10/105015

Piezoelectric MEMS resonators based on ultrathin epitaxial GaN heterostructures on Si

P Leclaire[1,2], E Frayssinet[1], C Morelle[2], Y Cordier[1], D Théron[2] and M Faucher[2]

[1] CRHEA-CNRS, UPR10, rue Bernard Grégory, 06560 Valbonne, France
[2] IEMN, CNRS UMR 8520, Avenue Poincaré, CS 60069, 59652 Villeneuve d'Ascq Cedex, France

E-mail: didier.theron@iemn.univ-lille1.fr

Received 8 April 2016, revised 8 July 2016
Accepted for publication 8 August 2016
Published 9 September 2016

CrossMark

Abstract
We present the first results for microelectromechanical (MEMS) resonators fabricated on epitaxial nitride semiconductors with thin buffers engineered for MEMS and NEMS applications. These results are used to assess the use of thin buffers for GaN MEMS fabrication. On a 700 nm thick AlGaN/GaN epilayer, a high tensile stress is observed to increase the resonant frequency. The electromechanical coupling efficiencies of integrated transducers are assessed and compared with previously obtained results on commercially available 2 μm thick epilayers used for power transistor applications. A 28 nm V^{-1} actuation efficiency is measured on the 700 nm thick structure which is slightly better than the one measured on the 2 μm buffer. The electrical response of a gateless detector designed as a piezoresistance is obtained and a gauge factor of 60 is estimated. These results show that material issues can be unlocked to exploit the potentialities of III-nitrides for NEMS applications.

Keywords: GaN, MEMS, resonators, heterostructure

(Some figures may appear in colour only in the online journal)

1. Introduction

Microelectromechanical systems (MEMS) are widely investigated for their applications in actuators and sensors of small dimensions and co-integrated with electronic functions. Among all the materials and technologies available, mainly silicon [1–3], but also quartz [4] and SiC [5, 6], GaN-based resonators have shown many advantages and could lead to a new generation of sensors [7]. Indeed, the piezoelectric properties of GaN combined with its thermal stability and chemical inertness are very interesting for addressing harsh environment applications [8, 9]. Furthermore, GaN benefits from its development on Si technology and the possibility of monolithic integration with AlGaN/GaN high electron mobility transistors (HEMTs) [10].

In MEMS resonators, the resonant frequency is given by $f_{\text{res}} = \sqrt{k/m}$, where k is the stiffness and m is the mass. When used for mass or force sensors, the phase variation near the resonance coming from additional mass or force is used as the detection signal. With the mechanical stiffness kept constant, it is given by $\Delta\varphi_n = -2Q_n\Delta f_{\text{res}}/f_{\text{res}} = -Q_n\Delta m/m$. Therefore, in order to enhance the detection sensitivity, high quality factors are required. Moreover, since stress is detected, small cross-section areas for applying the force will result in greater stress variation. Downscaling MEMS resonators will therefore enhance their sensitivity.

The first MEMS resonators based on III-nitrides on Si substrates were developed on epitaxial layers currently available at that time and optimized for RF power figures of merit. On silicon substrates, the standard buffer thicknesses are in the range of 2–5 μm. With buffer thickening, the dislocation density can be reduced to as low as 1–2 $\times$ 10^9 cm^{-2} [11] and the AlGaN/GaN heterostructure mobility can be increased up to 2100 cm^2 V^{-1} s^{-1} with an electron density of about 9 $\times$ 10^{12} cm^{-2} [12].

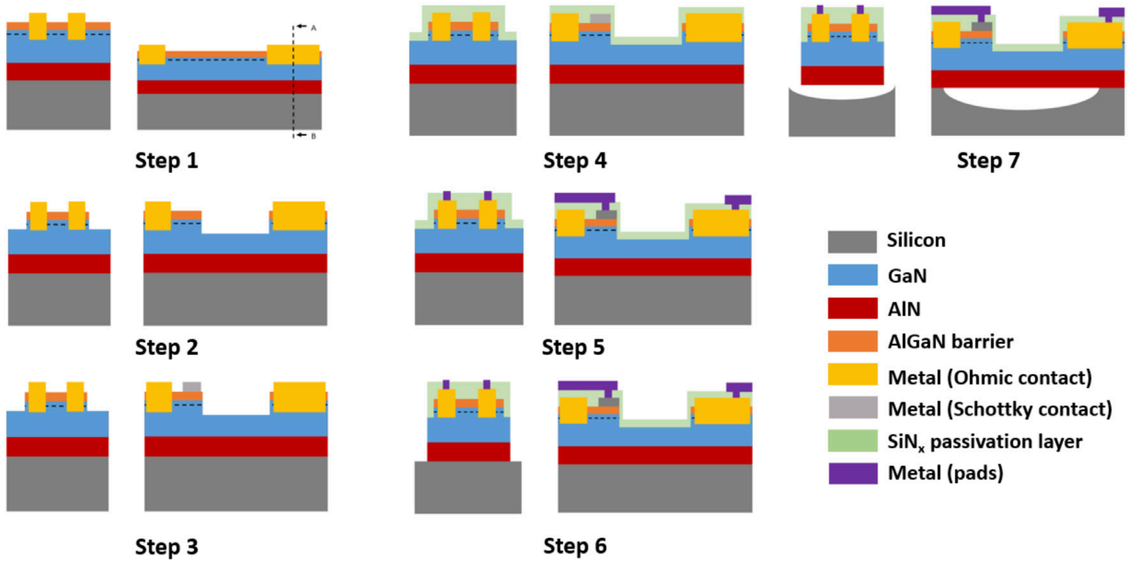

Figure 1. Process flow for the GaN MEMS resonator. For each step the side view A–B is shown on the left. Step 1: ohmic contact deposition and annealing. Step 2: definition of the 2DEG path using mesa isolation. Step 3: Schottky contact of Ni/Al/Ni metal stack defined by lift-off. Step 4: deposition, patterning of 50 nm of SiN passivation layer. Step 5: deposition of Ti/Au contact pads. Step 6: GaN etching. Step 7: resonator release with XeF_2 etching of the Si substrate under the GaN beam.

The fabrication of small-size resonators (NEMS) with good performance requires addressing the growth of thin structures. However, reducing the epitaxial layer thickness will result in an increase of the threading dislocation density and a degradation of electrical properties. In a previous work [13] we targeted having AlGaN/GaN heterostructures with electron mobility (μ) and electron density (n_s) higher than 1000 cm^2 V^{-1} s^{-1} and 5×10^{12} cm^{-2} respectively. We demonstrated the growth of AlGaN/GaN heterostructures on a GaN (500 nm)/AlN (200 nm) buffer with the expected trade-off between structural, mechanical and electrical properties. In the present work, we demonstrate MEMS resonators fabricated on such an AlGaN/GaN heterostructure grown on a 700 nm thin buffer. For convenient comparison with resonators realized on 2 μm thick layers, MEMS resonators were fabricated with similar dimensions on both wafers. The resonant frequency and piezoelectric actuation were investigated and compared with resonators fabricated on 2 μm thick layers purchased from EpiGaN.

2. Methods

2.1. Growth

An epitaxial AlGaN/GaN HEMT structure was grown by metal organic chemical vapor deposition on 2 inch Si (1 1 1) substrates in a Thomas Swan close-coupled showerhead reactor [11]. Trimethylaluminum and trimethylgallium were used as group III precursors and ammonia as a group V precursor. A 30 nm low-temperature AlN seed layer was first grown at 950 °C followed by 170 nm of AlN grown at 1140 °C. Then, a 500 nm GaN buffer was directly grown without any intermediate layer at about 1000 °C. A HEMT active layer was then grown on the GaN-on-Si buffer and was composed of a 3 nm GaN cap layer, a 20 nm AlGaN barrier with a 26% (±1%) Al content, as determined by x-ray diffraction (XRD), and a 1.5 nm AlN spacer. The dependence of the final average stress of the GaN layers was mainly controlled by the GaN thickness and nucleation layer structure. Using AlN or AlN/GaN/AlN stress-mitigating layers will result in either a tensile or a compressive layer [8, 14]. Here for thin-layer growth, we used AlN layers. This heterostructure exhibited an electron density of about 9×10^{12} cm^{-2} and a mobility of 1320 cm^2 V^{-1} s^{-1}.

2.2. Technological process

Doubly clamped GaN resonators 440 μm long and 40 μm wide were processed on 700 nm thin buffers on the basis of the GaN resonator fabrication process reported in [15]. Seven mask levels were used (figure 1) and e-beam lithography was used for convenience and easy design modification. The fabrication of GaN resonators consisted of processing transducers first, and then defining and releasing the mechanical parts. The process started with the deposition of a Ti/Al/Ni/Au metal stack of a total thickness of 350 nm which was patterned by lift-off and annealed for 30 s at 850 °C. These ohmic contacts were used at both sides of the resonator. On the actuator side, they were used as a path to connect the two-dimensional electron gas (2DEG) that was used as a back electrode. On the detector side, they defined the piezoresistance contacts. These contacts were designed in order to obtain a total resistance of about 100 Ω. Mesa isolation was performed by etching the active layers with Cl_2/Ar plasma. The next step consisted in fabricating the actuator top electrode by depositing a Ni/Al/Ni Schottky contact by lift-off. On the actuator, the GaN cap and the AlGaN barrier layer of the HEMT structure separated the top and bottom electrodes. For optimizing the actuation efficiency of the fundamental mode, the Schottky contact on the beam was designed in order to be located where the stress was the highest for that mode,

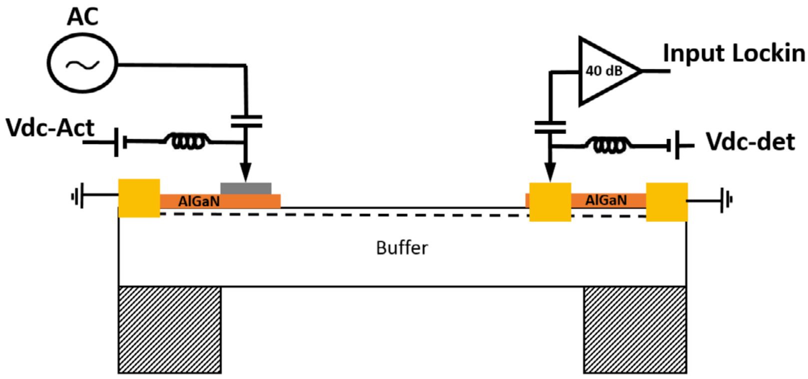

Figure 2. Electrical measurement setup used to characterize the resonator response at room temperature and under atmospheric pressure.

which was theoretically on the beam near the anchor [15]. Then, in order to protect the transducers and ensure surface passivation, a 50 nm Si_3N_4 layer was deposited by plasma-enhanced chemical vapor deposition at 340 °C. After opening passivation, Ti/Au coplanar metal pads were deposited. Then, the MEMS mechanical structure was patterned by etching the whole GaN epilayer by Cl_2/Ar plasma in an inductively coupled plasma etching reactor. Finally, the resonator was released by XeF_2 dry etching of the silicon substrate under the beam. Because of the relatively important beam width, the beam anchor point was slightly under-etched. This fabrication process induced a deviation from the design that resulted in a 20 μm shift of the anchoring points and an increase of the effective beam length.

2.3. Measurement setup

The test of GaN MEMS devices involved optical and AC electrical measurements performed at room temperature and under atmospheric pressure.

First, Doppler vibrometry laser measurement was used to determine the mechanical mode frequencies and in particular evaluate the vibration amplitude and quality factor of the first flexural mode. The vibrometer laser spot was thus located on the GaN beam where the amplitude of the studied mode was the largest. A sinusoidal signal of amplitude $V_{ac} = 1\,V$ with a DC offset of $-2\,V$ was supplied to the Schottky actuator with electrical ground–signal–ground probes. In order to evaluate the performance of the devices fabricated on a thin buffer, the measurement results were compared between two devices named sample Ref and sample A. The first one (sample Ref) was fabricated on commercially available AlGaN/GaN heterostructures with a 2 μm thick buffer and dimensions ($L \times W \times T$) of 400 μm $\times$ 20 μm $\times$ 2 μm [15]. The second one was fabricated on a 700 nm downscaled buffer and showed dimensions ($L \times W \times T$) of 440 μm $\times$ 40 μm $\times$ 0.7 μm (sample A).

Second, the electrical response of the detector was then measured using coplanar probes. The characterization setup is shown in figure 2. The actuation and detection transducers were DC biased using a Keithley 2612 and a lock-in amplifier (HF2LI, Zurich Instruments) was used to apply and measure AC signals. Two bias tees were used to combine the AC and DC signals. The first one was used to set a negative DC bias to the actuator for preventing the degradation of the Schottky contact with direct current while applying the AC signal. The second bias tee allowed biasing the piezoresistance detector and recording the resonator response on the input port of the lock-in. A 40 dB amplifier with a 10 MHz bandwidth was used to amplify the device response.

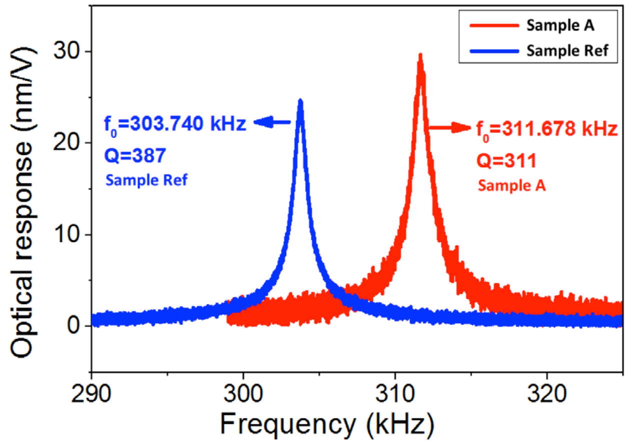

Figure 3. Characterization of the resonator motion by Doppler vibrometry measurement under atmospheric pressure and at room temperature (293 K). Here the first flexural mode resonances are shown. Piezoelectric excitation is provided by the Schottky diode with a DC bias V_{dc} of $-2\,V$ and an AC bias V_{ac} of 1 V amplitude.

3. Results and discussion

3.1. Resonant frequency

The first flexural mode resonances of the two resonators measured by Doppler vibrometry are shown in figure 3. A minimum of 1000 data points were used for scanning the frequency. The quality factors of samples A and Ref measured in air were 311 and 387 respectively. To estimate the reproducibility of the measurements and devices, a few resonators with the same dimensions were measured on sample Ref. The dispersion in the resonant frequency and quality factor was in the range of a few percent. In order to analyze the value of the resonant frequency, we used its analytical expression deduced from the Rayleigh method and based on energy conservation. According to [16] it can be approximated as a function of the pre-stress σ by the following equation:

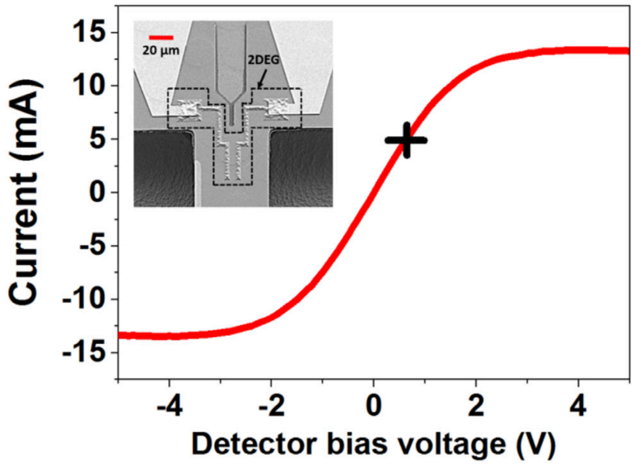

Figure 4. *I–V* measurement of the piezoresistive detector. The applied voltage varies from -5 V to 5 V. The black cross shows the bias point used for motion detection. Inset: SEM view of the measured transducer. The dotted line follows the mesa edge.

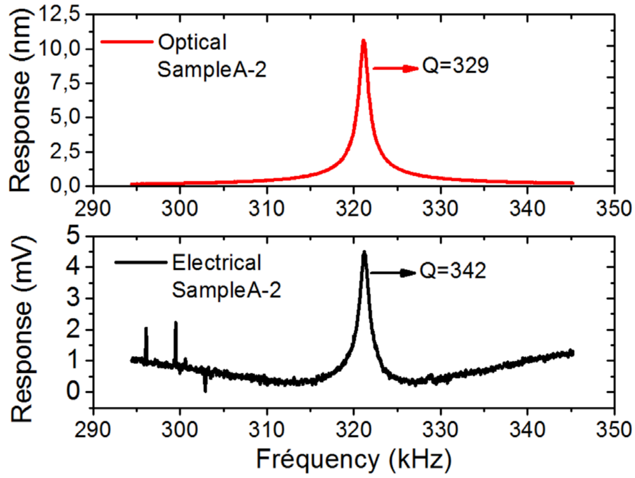

Figure 5. Experimental vibration spectra of the first flexural mode at ambient conditions on sample A. The actuation voltage is $V_{dc} = -2$ V with a 1 V V_{ac} amplitude. Top: Doppler vibrometry measurement with the laser spot located on the detector. Bottom: piezoresistance response, measured with 40 dB amplification for the same device and the same actuation bias. The piezoresistance bias is 900 mV.

$$f_{n,\sigma} = \frac{k_n^2 T}{2\pi L^2}\sqrt{\frac{E_{\text{eff}}}{12\rho}}\sqrt{1+\gamma_n\frac{\sigma L^2}{E_{\text{eff}}T^2}} \qquad (1)$$

where n is the mode index, k_n is the mode-dependent eigenvalue equal to 4.73, 7.85, …, $(n + 1/2)\pi$, ρ is the average beam mass density, E_{eff} is the effective Young's modulus, and γ_n is a mode- and stress-dependent coefficient [17, 18].

In a previous work [13] we have shown that Young's modulus does not significantly depend on the buffer thickness and exhibits an average value of 260 GPa. We also expect to have an average mass density similar for the 2 μm and 0.7 μm layers because the 0.7 μm layers show good crystalline qualities as attested by XRD. Therefore, differences in resonant frequencies are mainly ascribed to the beam dimensions and average prestress. From our measurements, sample A exhibits a resonant frequency of 8 kHz higher than that of sample Ref although it is 40 μm longer and 2.8 times as thin. According to equation (1), we deduce a high tensile residual stress for both epitaxial layers. In the present case, the residual stress is found to be tensile with 440 MPa for sample A and 295 MPa for sample Ref. This higher residual stress σ for sample A than for sample Ref is ascribed to the transition between the Si substrate and GaN which is made of a single AlN layer for the 700 nm thick buffer. Indeed, in such a thin structure, there is no AlGaN interlayer that introduces an intrinsic compressive stress in order to balance the tensile stress induced by the large difference in thermal expansion coefficient between the epilayers and the Si substrate [13]. The measured quality factors are attributed to air damping and are in the same range as those expected using viscous damping calculation in air [19]. In this model, the quality factor only slightly increases with frequency. This may explain the low $f \cdot Q$ product of our devices.

3.2. Actuation

The actuator efficiencies η_{act} of sample A and Ref are 28 nm V^{-1} and 25 nm V^{-1} on average respectively. Due to the vibrometer laser spot radius, which is about 5 μm, and to the error made while placing the laser spot on the beam, the amplitude has been obtained with an error of about 5–8 nm. For these reasons, it is hard to conclude any improvement or damage to the actuation efficiency due to the use of a thinner buffer. However, the measured values are about three to five times as low as predicted by equation (2) [20] that gives 130 nm V^{-1} for sample Ref and 78 nm V^{-1} for sample A:

$$\eta_{\text{act}} = -e_{31\text{AlGaN}}\frac{1}{2}\frac{W_{\text{act}}}{W}\frac{Q}{4\pi^2 f_1^2\rho}\frac{U'(L_{\text{act}})U(x_r)}{\int_0^L U^2(x)\mathrm{d}x} \qquad (2)$$

where $e_{31\text{AlGaN}}$ is the piezoelectric coefficient (-0.4 C m^{-2}), W_{act} and L_{act} are the actuator electrode width and length respectively, and $U(x)$ is the shape of the vibration mode. Here mode shape reduction at x_r has been done considering the vibration beam equivalent to a point mass located at position $x_r = L/2$. This discrepancy between the measurement and the model is not fully understood yet. This has been observed in other work [21] and attributed to several possible effects related to the structural and electronic properties of the actuator such as the under-etching of the anchors during beam release etching, the presence of a top metallic electrode or the 2DEG resistance. In our case, we observe that devices with the same dimensions and similar resonant frequencies and quality factors could present significantly different actuation factors (up to a factor of 8). Therefore, we do not attribute the low actuation efficiency to the dimensions or to the under-etching of the beam because this would also modify the resonant frequency. Moreover, under our biasing conditions, we do not expect the 2DEG to be depleted. First, we obtain the same values using a DC offset of -1 V and, second, the pinch-off voltage measured on a HEMT fabricated on similar structures is typically around -4 V. We therefore suggest that the actuator may be impacted by intrinsic parasitic effects.

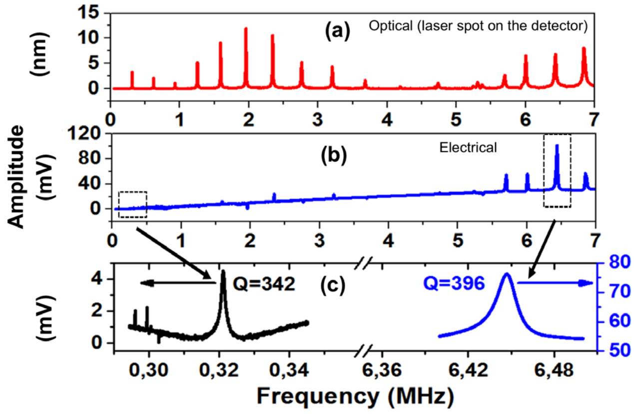

Figure 6. Optical and electrical response amplitude of a 440 μm long and 40 μm wide doubly clamped beam on a 700 nm thin buffer up to 7 MHz. (a) Optical Doppler vibrometry signal. (b) Electrical detection signal. (c) Zoom of the electrical signal for the first and 16th flexural mode. The actuation voltage is $V_{act} = -2 + 1 \cdot \cos(\omega t)$ V and the detector is DC biased at 900 mV.

3.3. Piezoresistive detection

Electrical detection of the thin layers has been performed by measuring the voltage amplitude variation of the output piezoresistance on sample A. In the past, we used an R-HEMT to detect the beam motion for better efficiency and intrinsic amplification of the detected signal [15]. The choice of a piezoresistance over an R-HEMT is due to the perspective of downscaling the device. Indeed, reducing the piezoresistance dimensions will be less difficult than reducing the R-HEMT ones because the R-HEMT requires keeping a gate and therefore occupies more space on the beam. In order to optimize the detected signal, the piezoresistance is located where the longitudinal stress is at its maximum, that is, on the beam near the anchor [15].

The *I*–*V* characteristic of the piezoresistance shows a linear behavior from -2V to 2V with a total resistance of 130 Ω, which is in good agreement with the 100 Ω aimed by design (figure 4). In order to stay in the linear region, a bias of 900 mV corresponding to a 5 mA current (black cross in figure 4) is chosen. Then, as previously, the actuator is biased with a -2V DC offset and a 1 V amplitude AC signal. The result of the electrical response was compared with vibrometry measurements on the same device under the same bias (figure 5). To measure the intrinsic detector efficiency, the laser spot was placed on the detector. For the first mode, the actual amplitude at the transducer was 10.6 nm. The obtained electrical efficiency, which we defined as the ratio between the electrical and the mechanical amplitudes, was 4.5 μV nm^{-1} after removal of the 40 dB amplification factor. In order to estimate the corresponding piezoresistive gauge factor ($G = \frac{\Delta R}{R}\frac{1}{\varepsilon_{ave}}$), we calculated the average strain ε_{ave} along the detector by solving the Euler–Bernoulli equation [18] for the first vibration mode and deduced a value of $G = 60$. This value was comparable with those of undoped silicon and β-SiC [22] but much lower than those of GaN cantilevers [23]. Additionally, we measured the Doppler vibrometry response and the electrical response of the resonator up to 7 MHz as shown in figure 6. The different high-frequency modes did not always show a large amplitude since the detection signal depended either on the laser position on the beam for Doppler vibrometry or on the detector length for electric detection. We first observed that the electrical response of the resonator increased above 5 MHz as compared to the Doppler vibrometry response. Second, contrary to the behavior of GaN MEMS resonators on a thick buffer [24], we observed an increase of the electrical response for high-frequency resonant modes (figure 6(b)). The highest amplitude of the electrical response was obtained for the 16th frequency resonant mode (figure 6(c)). The amplitude rose from 4.5 mV for the first mode located around 320 kHz up to 76 mV for the 16th mode located around 6.45 MHz. Additionally, the difference between the peak amplitude and the background signal of the 16th mode was five times as large as the one measured on the first mode despite the enhanced capacitive coupling between the actuator and detector that led to an increase of the background signal from 1 mV to 55 mV. For the 16th mode, the obtained transduction efficiency was 125 μV nm^{-1}, which is 27 times as high as that for the first mode. This value indicates that the gauge factor deduced at low frequency from the first mode might be strongly improved as expected from A Talukdar's results [23, 25].

To understand this phenomenon, we consider that the detection mechanism mainly involves the 2DEG sheet carrier density variation due to the local compensation of the piezoelectric charge mechanically induced by beam vibration [15]. Thus the detected signal amplitude depends on the piezoelectric properties of the GaN as well as the electronic properties of the 2DEG. However, the specificity of a thin buffer is to exhibit (i) a very high density of threading dislocations and (ii) a very small thickness of a fully relaxed GaN buffer [13]. Therefore, dislocations that act as electron/hole recombination centers [26] and electron traps [27] are close to the 2DEG. At low frequency where these traps can be charged and discharged, they will compete with the 2DEG to compensate the piezoelectric charge induced by the beam motion. One possible origin of the lack of detection at low frequency may therefore be the high density of traps located in the buffer. Moreover, Miller *et al* have reported that the time constant of the trap states in AlGaN/GaN devices is about 1 μs [28]. This result is consistent with our measurements where the detector efficiency increases for resonant frequencies higher than 1.2 MHz.

4. Conclusion

In conclusion, we have used an AlGaN/GaN heterostructure grown on Si with a 700 nm buffer layer to fabricate MEMS resonators with piezoelectric actuation and piezoresistive detection. These devices compared to similar ones fabricated on 2 μm thick buffers exhibit higher residual stress as deduced from their higher resonant frequencies. Their actuation efficiency is similar but may still be improved as expected from theoretical prediction. Although the dislocations present near the 2DEG seem to be responsible for a drop of the detector efficiency at low frequency, the use of resonant frequencies above 5 MHz leads to a recovered response. Further improvement in thin GaN on Si epitaxial layers may yield excellent detection efficiency in a larger frequency range. These results are very encouraging from the perspective of NEMS resonators based on GaN on Si technology.

Acknowledgments

The authors would like to thank Dr V Zhang for his helpful discussions. We acknowledge financial support from 'Investissements d'Avenir' GaNeX (ANR-11-LABX-0014), the French Renatech network and the ASTRID project AMGaSi (ANR-11-ASTR-0037) funded by the French National Research Agency.

References

[1] Ollier E *et al* 2012 Ultra-scaled high-frequency single crystal silicon NEMS resonators and their front end co-integration with CMOS for high sensitivity applications *25th IEEE Int. Conf. on (MEMS) Micro Electro Mechanical Systems* pp 1368–71

[2] Minne S C, Manalis S R and Quate C F 1995 Parallel atomic force microscopy using cantilevers with integrated piezoresistive sensors and integrated piezoelectric actuators *Appl. Phys. Lett.* **67** 3918–20

[3] Howe R T 1983 Polycrystalline silicon micromechanical beams *J. Electrochem. Soc.* **130** 1420–3

[4] Le Traon O, Janiaud D, Pernice M, Masson S, Muller S and Tridera J-Y 2006 A new quartz monolithic differential vibrating beam accelerometer *IEEE Plans, Position Location and Navigation Symp.* pp 6–15

[5] Boubekri R *et al* 2014 Electrothermally driven high-frequency piezoresistive SiC cantilevers for dynamic atomic force microscopy *J. Appl. Phys.* **116** 054304

[6] Kermany A R, Brawley G, Mishra N, Sheridan E, Bowen W P and Iacopi F 2014 Microresonators with *Q*-factors over a million from highly stressed epitaxial silicon carbide on silicon *Appl. Phys. Lett.* **104** 081901

[7] Popa L C and Weinstein D 2013 2DEG electrodes for piezoelectric transduction of AlGaN/GaN MEMS resonators *2013 Joint European Frequency and Time Forum and Int. Frequency Control Symp., EFTF/IFC 2013* pp 922–5

[8] Rais-Zadeh M, Gokhale V J, Ansari A, Faucher M, Théron D, Cordier Y and Buchaillot L 2014 Gallium nitride as an electromechanical material *J. Microelectromech. Syst.* **23** 1252–71

[9] Cimalla V, Pezoldt J and Ambacher O 2007 Group III nitride and SiC based MEMS and NEMS: materials properties, technology and applications *J. Phys. D: Appl. Phys.* **40** 6386–434

[10] Ansari A, Gokhale V J, Roberts J and Rais-Zadeh M 2012 Monolithic integration of GaN-based micromechanical resonators and HEMTs for timing applications *IEEE Int. Electron Devices Meeting (IEDM)* pp 15.5.1–15.5.4

[11] Frayssinet E, Cordier Y, Schenk H P D and Bavard A 2011 Growth of thick GaN layers on 4 in. and 6 in. silicon (1 1 1) by metal-organic vapor phase epitaxy *Phys. Status Solidi* **8** 1479–82

[12] Rennesson S, Lecourt F, Defrance N, Chmielowska M, Chenot S, Lesecq M, Hoel V, Okada E, Cordier Y and De Jaeger J-C 2013 Mobility heterostructures for high-power / frequency performances *IEEE Trans. Electron Devices* **60** 3105–11

[13] Leclaire P, Chenot S, Buchaillot L, Cordier Y, Théron D and Faucher M 2014 AlGaN/GaN HEMTs with very thin buffer on Si (1 1 1) for nanosystems applications *Semicond. Sci. Technol.* **29** 115018

[14] Krost A and Dadgar A 2002 GaN-based optoelectronics on silicon substrates *Mater. Sci. Eng.* B **93** 77–84

[15] Faucher M, Cordier Y, Werquin M, Buchaillot L, Gaquière C and Théron D 2012 Electromechanical transconductance properties of a GaN MEMS resonator with fully integrated HEMT transducers *J. Microelectromech. Syst.* **21** 370–8

[16] Brueckner K, Niebelschuetz F, Tonisch K, Foerster C, Cimalla V, Stephan R, Pezoldt J, Stauden T, Ambacher O and Hein M A 2011 Micro- and nano-electromechanical resonators based on SiC and group III-nitrides for sensor applications *Phys. Status Solidi* **208** 357–76

[17] Bouwstra S and Geijselaers B 1991 On the resonance frequencies of microbridges *TRANSDUCERS '91 1991 Int. Conf. Solid-State Sensors Actuators* pp 538–42

[18] Brueckner K, Cimalla V, Niebelschütz F, Stephan R, Tonisch K, Ambacher O and Hein M A 2007 Strain- and pressure-dependent RF response of microelectromechanical resonators for sensing applications *J. Micromech. Microeng.* **17** 2016–23

[19] Aoust G, Levy R, Bourgeteau B and Traon O Le 2016 Acoustic damping on flexural mechanical resonators *Sensors Actuators* A **238** 158–66

[20] Ben Amar A *et al* 2012 Bias dependence of gallium nitride micro-electro-mechanical systems actuation using a two-dimensional electron gas *Appl. Phys. Express* **5** 067201

[21] Brueckner K, Niebelschuetz F, Tonisch K, Michael S, Dadgar A, Krost A, Cimalla V, Ambacher O, Stephan R and Hein M A 2008 Two-dimensional electron gas based actuation of piezoelectric AlGaN/GaN microelectromechanical resonators *Appl. Phys. Lett.* **93** 173504

[22] Shor J S, Goldstein D and Kurtz A D 1993 Characterization of *n*-type β-SiC as a piezoresistor *IEEE Trans. Electron Devices* **40** 1093–9

[23] Talukdar A, Qazi M and Koley G 2012 High frequency dynamic bending response of piezoresistive GaN microcantilevers *Appl. Phys. Lett.* **101** 252102

[24] Faucher M, Ben Amar A, Grimbert B, Brandli V, Werquin M, Buchaillot L, Gaquíere C, Théron D, Cordier Y and Semond F 2011 GaN: a multifunctional material enabling MEMS resonators based on amplified piezoelectric detection *2011 Joint European Frequency and Time Forum and Int. Frequency Control Symp. (EFTF/IFC)* pp 1–5

[25] Talukdar A, Faheem Khan M, Lee D, Kim S, Thundat T and Koley G 2015 Piezotransistive transduction of femtoscale displacement for photoacoustic spectroscopy *Nat. Commun.* **6** 7885

[26] Morrison S R 1956 Recombination of electrons and holes at dislocations *Phys. Rev.* **104** 619–23

[27] Wong Y-Y, Chang E Y, Yang T-H, Chang J-R, Ku J-T, Hudait M K, Chou W-C, Chen M and Lin K-L 2010 The roles of threading dislocations on electrical properties of AlGaN/GaN heterostructure grown by MBE *J. Electrochem. Soc.* **157** H746

[28] Miller E J, Dang X Z, Wieder H H, Asbeck P M, Yu E T, Sullivan G J and Redwing J M 2000 Trap characterization by gate-drain conductance and capacitance dispersion studies of an AlGaN/GaN heterostructure field-effect transistor *J. Appl. Phys.* **87** 8070